A Modified VSG Control Scheme With Virtual Resistance to Enhance Both Small-Signal Stability and Transient Synchronization Stability

Shimiao Chen, Yao Sun, Hua Han, Siqi Fu, Shihan Luo, and Guangze Shi

***Abstract*—The existing studies show that the virtual resistance scheme has positive effects on synchronous resonance suppression but negative effects on transient synchronization stability of virtual synchronous generator (VSG). To address this contradiction, this article proposes a modified VSG control scheme. The basic idea is that the virtual active power at virtual PCC, instead of real active power, is introduced as the power feedback into the control loop. Then, the effect of virtual resistance on transient stability can be equivalent to that of grid resistance, which improves transient stability. Besides, a proportion–integral controller is added at the forward loop to control the real active power to track the power reference. Compared with the existing VSG control methods, the modified VSG control scheme can well solve the conflict caused by virtual resistance between small-signal stability and transient stability. The effectiveness and superiority of the proposed method are verified by control hardware-in-loop experimental results.**

***Index Terms*—Grid-forming control, synchronous resonance (SR), transient synchronization stability, virtual resistance, virtual synchronous generator (VSG).**

I. Introduction

POWER grids are interfaced by more and more inverter-interfaced distribution generators (IIDGs) [1], [2]. The grid-forming converters control based on IIDG, among the various available control strategies, is deemed to be the most promising solution for low-inertia power systems [3], [4], [5]. Virtual synchronous generator (VSG) is one of the typical grid-forming control methods [6], [7], [8]. VSG control introduces the swing equation of SGs into the control algorithm to emulate the inertia and damping characteristics of the synchronous generator and provides grid-friendly virtual inertia to ensure frequency stability [9].

Virtual impedance or virtual resistance technology has been widely used on VSG-IIDGs [4], [10], [11], [12], [13], [14], [15], [16]. Substantial efforts have been devoted to the application of virtual impedance for various purposes, including reactive power-sharing enhancement in microgrids [11], current limitation [12], transient oscillations damping, and small-signal stability improvement [13], [14], [15]. In the aspect of small-signal stability improvement, virtual resistance is introduced to damp synchronous resonance (SR) [16], [17], [18]. SR is one of the typical small-signal stability issues of grid-forming control converters [19]. A pair of conjugate open-loop poles at $-R/L \pm j\omega_g$ will be introduced and lead to potential instability, especially in a system with a low *R*/*X* ratio. Compared with adding a real resistor to the output of the IIDG, virtual resistance is effective for SR suppression without extra power loss.

Even though the above studies explored the benefits of virtual resistance in many aspects, virtual resistance jeopardizes the transient synchronization stability of VSG [20]. The transient stability represents the ability of the VSG–IIDG to maintain synchronization with the grid under large disturbances. In [21], the phase-portrait method is used to analyze the transient stability of the four typical grid-forming control schemes. And the conclusion has been drawn that smaller virtual inertia *J* and larger damping coefficient *D* conduces to the transient stability of VSG–IIDG. To further improve the transient stability of VSG, methods to modify the active power control loop, like the transient damping method [22], [23], [24], codesign control parameters method [25], and mode-adaptive-switching method [26], [27] have been proposed. The influence of the reactive power control loop of VSG is also studied in [28]. It analyzed the deterioration of transient stability brought by the reactive power control loop with the Lyapunov direct method. In [29] and [30], the VSG reactive control loop is modified to enhance transient stability. Besides, the virtual impedance cascading with HPF (high-pass filter), also known as the transient virtual impedance [10], [16], [34], [35], can help improve transient stability, but its performance is limited. These methods can be summarized in Table I. Although so many enhancement methods have been proposed recently, the conflict between small-signal stability and transient synchronization stability of VSG introduced by virtual resistance still needs to be solved.

This article focuses on the conflict caused by virtual resistance between SR suppression in small-signal stability and transient synchronization stability of VSG. The contribution is summarized as follows:

Manuscript received 19 June 2022; revised 22 November 2022; accepted 30 January 2023. Date of publication 7 February 2023; date of current version 10 March 2023. This work was supported in part by the Science and Technology Innovation Program of Hunan Province under Grant 2020RC4002, and in part by the National Natural Science Foundation of China under Grants 62125308, 62192754, 61933011, and 52177205. Recommended for publication by Associate Editor H. Wang. *(Corresponding author: Yao Sun.)*

The authors are with the School of Automation, Central South University, Changsha 410017, China (e-mail: 214601009@csu.edu.cn; yaosuncsu@gmail.com; hua_han@126.com; siqi_fu_csu@csu.edu.cn; shihanluo@163.com; 16414986@qq.com).

Color versions of one or more figures in this article are available at https://doi.org/10.1109/TPEL.2023.3243025.

Digital Object Identifier 10.1109/TPEL.2023.3243025

TABLE I
EXISTING TRANSIENT STABILITY ENHANCEMENT METHODS FOR VSG—IIDG

Methods	Proposals	Influence of R_v
Modify the control loop	•Transient damping [22-24] •Mode-switching [26] •Adaptive virtual inertia [27] •Modify Q-V control loop [29-30]	Negative to transient stability
Change the power reference	•Reducing P reference [20,28,31] •Increasing Q reference [32]	Negative to transient stability
Co-design control parameters	•Coordinate J and D [21] •Optimal Damping Design [25]	Negative to transient stability
Output impedance optimization	•Adaptive virtual resistance [33]	Negative to transient stability
	•Transient virtual impedance cascading with HPF [16, 34, 35]	Limited improvement in transient stability

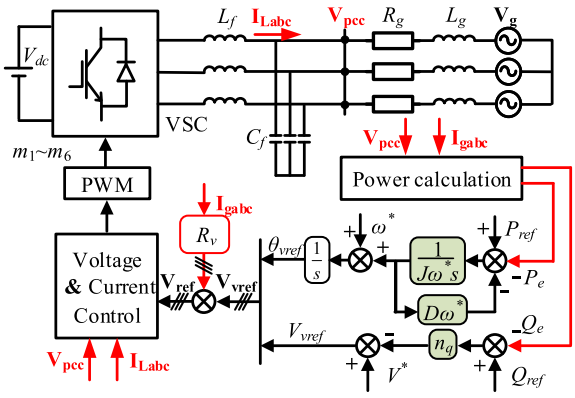

Fig. 1. General structure of the three-phase VSG with virtual resistance.

1) A simple but effective modified VSG control scheme is proposed to address the conflict we studied. Virtual active power replaces real active power in the control loop and enhances both small-signal stability and transient synchronization stability with the existence of virtual resistance.
2) Comprehensive and valid proof of the effectiveness of the proposed method is presented. The proposed method extends the VSG control structure and can be cooperated with other enhancement methods to further improve the transient synchronization stability while the required functions of grid-forming control remain.

The rest of this article is organized as follows. In Section II, the conflict caused by virtual resistance between small-signal stability and transient synchronization stability of VSG is reviewed. Section III presents the modified VSG scheme in detail. Control hardware-in-loop (CHIL) experimental results are provided in Section IV. Conclusions are presented in Section V.

II. EFFECTS OF VIRTUAL RESISTANCE ON SMALL-SIGNAL STABILITY AND TRANSIENT SYNCHRONIZATION STABILITY

A. VSG System Description

Fig. 1 depicts the general structure of the three-phase grid-connected VSG system. Virtual resistance R_v is introduced for

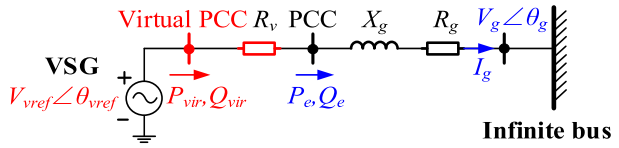

Fig. 2. Equivalent circuit of the VSG with virtual PCC and virtual resistance.

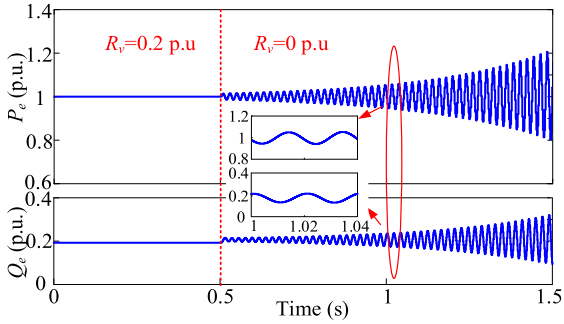

Fig. 3. Response curves of P_e and Q_e with different virtual resistance R_v.

SR suppression, and the voltage reference is changed to $\boldsymbol{V}_{\mathbf{ref}} = \boldsymbol{V}_{\boldsymbol{vref}} - R_v \boldsymbol{I}_{\boldsymbol{gabc}}$. R_g and L_g represent the grid resistance and inductance, respectively. $\boldsymbol{V}_g$, $\boldsymbol{V}_{\mathbf{pcc}}$, $\boldsymbol{I}_{gabc}$, and $\boldsymbol{I}_{Labc}$ are the space vectors to represent the grid voltage, the PCC voltage, the PCC current, and the inductor current, respectively.

The transient stability of the VSG is mainly determined by the outer power control loops [21]. Besides, this article only focuses on the large disturbances which do not provoke the overcurrent limit control [26], [33], [36].

The outer power control loop of VSG can be expressed as follows:

$$J\omega^* \frac{\mathrm{d}\omega}{\mathrm{d}t} = P_{\mathrm{ref}} - P_e - D\omega^*(\omega - \omega^*) \tag{1}$$

$$V_{v\mathrm{ref}} = V^* - n_q(Q_{\mathrm{ref}} - Q_e) \tag{2}$$

where J, D, and n_q represent the virtual inertia constant, damping coefficient, and Q-V loop coefficient, respectively. P_{ref}, Q_{ref}, and P_e, Q_e are the power reference and output power at the PCC, respectively. ω^* and ω are the frequency reference and output voltage angular frequency, respectively, and V^* and $V_{v\mathrm{ref}}$ are the voltage normal amplitude and voltage amplitude, respectively.

B. Effects of Virtual Resistance on Small-Signal Stability

Fig. 2 shows the equivalent circuit of the VSG with virtual resistance. Assuming the grid impedance is inductive, the dynamic small-signal model of P_e and Q_e can be expressed as

$$\Delta P_e = G_{P\delta} \Delta\delta_{v\mathrm{ref}} \tag{3}$$

$$\Delta Q_e = G_{QV} \Delta V_{v\mathrm{ref}} \tag{4}$$

where $G_{P\delta}(s)$ and $G_{QV}(s)$ are shown in Appendix.

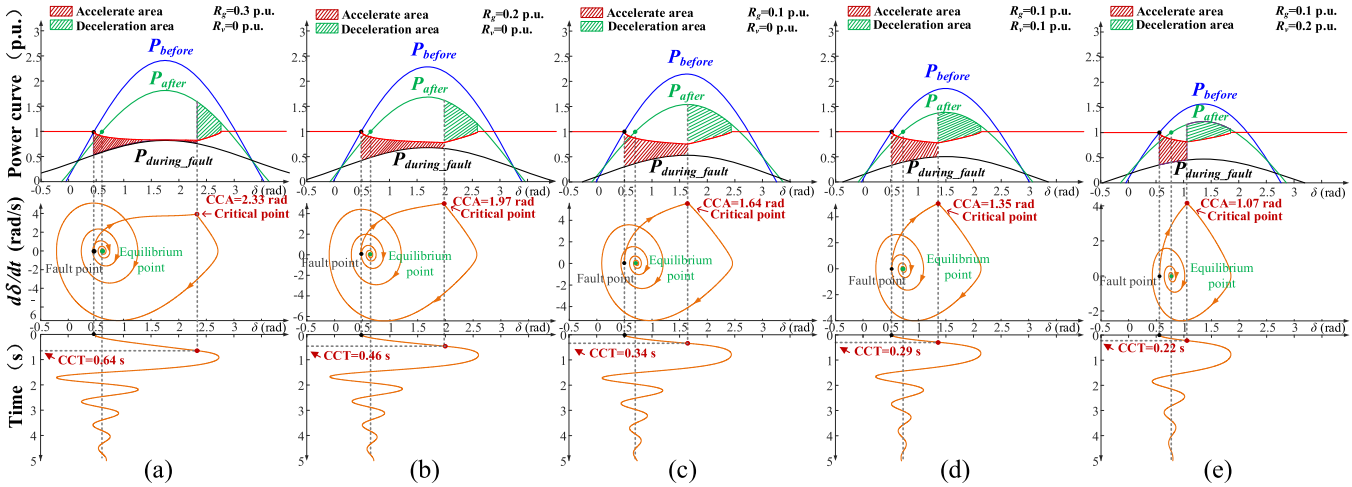

Fig. 4. Power angle curve of $P_e - \delta_{v\mathrm{ref}}$, phase portrait, and transient response with different R_v and R_g.

The VSG open-loop transfer functions from output power to power reference can be derived as

$$G_{P\_ol}(s) = \frac{1}{s\omega^*(Js+D)} G_{P\delta}(s) \tag{5}$$

$$G_{Q\_ol}(s) = n_q G_{QV}(s) \tag{6}$$

where $G_{P\cdot ol}(s)$ and $G_{Q\cdot ol}(s)$ represent the open-loop transfer function of $\Delta P_e(s)/\Delta P_{\mathrm{ref}}(s)$ and $\Delta Q_e(s)/\Delta Q_{\mathrm{ref}}(s)$, respectively.

It is reported that a pair of conjugate open-loop poles will be introduced and may lead to potential instability [16], [17], [18] and adding the virtual resistance can help to solve this issue [20]. Fig. 3 shows the response of P_e and Q_e when R_v decreases from 0.2 p.u. to 0 at 0.5 s. Virtual resistance can effectively increase the system stability from the small-signal stability perspective.

C. Effects of Virtual Resistance on Transient Synchronization Stability

The transient stability issue is induced by the dynamic of the power angle under large disturbance [23]. Without loss of generality, we mainly analyze the transient stability problem with no equilibrium point [26]. The system can recover to be stable if the disturbance is cleared before the critical clear time (CCT). CCT and critical clear angle (CCA) are utilized as the transient stability indicators.

According to expanded equal area criterion and the phase portrait, Fig. 4 is plotted to further illustrate the influence of virtual resistance R_v and grid resistance R_g on transient stability. An inverse time integral-based approach is applied to obtain a more accurate CCT and a less conservative transient stability boundary [5]. From Fig. 4, the effects of R_v and R_g on transient synchronization stability are opposite. CCT and CCA increase with the increase of R_g, while larger R_v results in the reduction of CCT and CCA. Therefore, the existence of R_v will jeopardize the transient synchronization stability of VSG, while R_g is conducive to transient stability.

D. Discussion

As discussed previously, the virtual resistance method can be adopted for SR suppression from a small-signal stability perspective. However, the existence of virtual resistance will inevitably lead to the deterioration of transient stability. Therefore, the conflict between small-signal stability and transient synchronization stability is urgent to be settled down.

III. Proposed Modified VSG Control Scheme With Virtual Resistance

A. Proposed Modified VSG Control Scheme

To address the conflict caused by virtual resistance, a modified VSG control scheme is proposed. The modified control scheme is shown in Fig. 5 and can be expressed as

$$\begin{cases} J\omega^* \frac{\mathrm{d}\omega}{\mathrm{d}t} = P_m - P_{\mathrm{vir}} + k \cdot \left[k_p(P_m - P_e) + k_i \int (P_m - P_e)\mathrm{d}t\right] \\ P_m = P_{\mathrm{ref}} - D\omega^*(\omega - \omega^*) \end{cases} \tag{7}$$

where P_{vir} represents the virtual active power at virtual PCC. P_e represents the real active power. P_m represents the input power reference after frequency feedback. k_p and k_i are the proportional coefficient and the integral coefficient of the PI (proportion–integral) controller. k takes the value of 0 or 1, which depends on the converter operating mode. The PI controller is designed to make the real active power P_e track the power reference P_{ref} in normal conditions ($k = 1$). In the fault conditions ($k = 0$), the PI controller is disconnected. The fault detection methods to trigger the value of k are not discussed in detail in this article, more detailed information can be referred to [23], [38], [39], [40].

The virtual active power P_{vir} is expressed as

$$P_{\mathrm{vir}} = \frac{3}{2}(V_{v\mathrm{ref}d} I_{gd} + V_{v\mathrm{ref}q} I_{gq}) \tag{8}$$

where $V_{v\mathrm{ref}d}$, $V_{\mathrm{ref}q}$, I_{gd}, and I_{gq} are the voltage $V_{v\mathrm{ref}}$ components and current I_g components in a rotating reference frame dq with the d-axis aligned with the grid voltage.

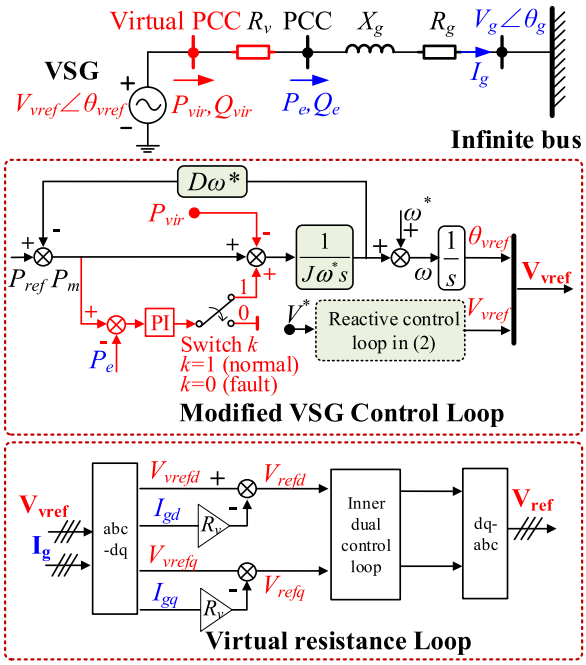

Fig. 5. Proposed modified VSG control with virtual resistance R_v.

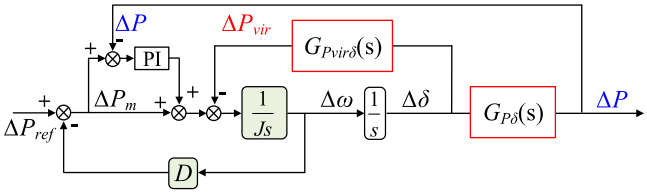

Fig. 6. Small-signal control block diagram of the modified VSG method with virtual resistance R_v.

Compared with other methods [20], [21], [22], [33], the key is that the virtual power $P_{\rm vir}$ is introduced to the active power control loop in (7) instead of the real power P_e. Then, the effect of virtual resistance R_v on transient stability can be equivalent to that of the grid resistance R_g. The small-signal stability and transient stability enhancement of the proposed modified VSG control scheme are analyzed as follows.

B. Small-Signal Stability Analysis

The small-signal control block diagram of the modified VSG with virtual resistance can be derived in Fig. 6. This analysis is based on the normal condition (the switch $k = 1$), which means the PI controller is connected. $G_{P{\rm vir}\delta}(s)$ is the small-signal transfer function of $P_{\rm vir}(s)/\delta(s)$, which is shown in the Appendix.

The bode diagram of the open-loop transfer function $\Delta P(\rm s)/\Delta P_{\rm ref}(\rm s)$ is shown in Fig. 7. With the increase of R_v, the resonance peak value is reduced effectively. Thus, the effectiveness of virtual resistance on SR suppression remains under the proposed modified VSG control. The small-signal stability is improved.

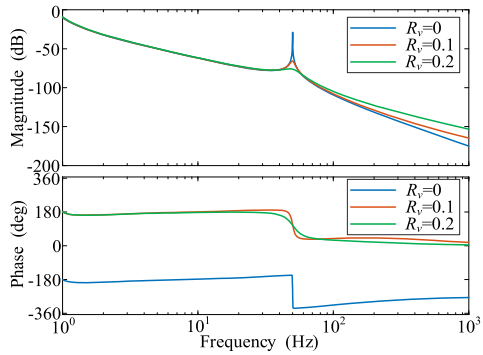

Fig. 7. Bode diagram of $\Delta P(\rm s)/\Delta P_{\rm ref}(\rm s)$ with $R_g = 0.05$ p.u. and $X_g = 1.5$ p.u.

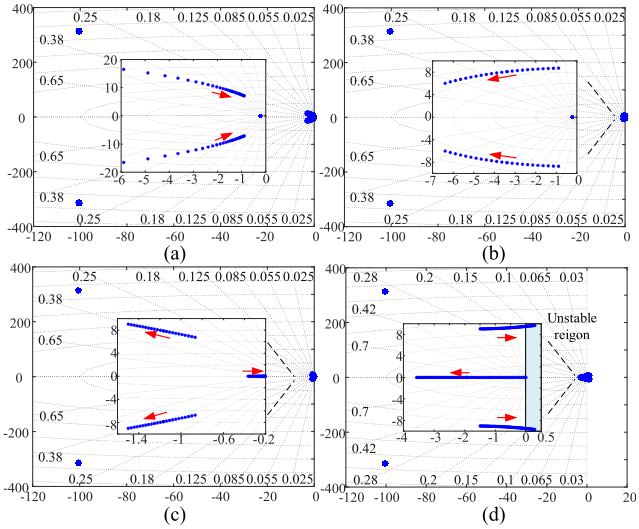

Fig. 8. Root locus (a) when J varies from 1 to 10; (b) when D varies from 1 to 10; (c) when k_p varies from 0.01 to 0.5; and (d) when k_i varies from 0.1 to 10.

To further analyze the influence of the rest control parameters on the small-signal stability, the root locus method is applied. Fig. 8(a) and (b) shows the root locus when J and D vary, which is similar to the conventional VSG control [8]. Fig. 8(c) and (d) shows the root locus when k_p and k_i vary. The existence of the integral term is unfavorable for small-signal stability. When the integral coefficient k_i is too large, a pair of closed-loop poles will move to the right region of the imaginary axis and lead to instability. Considering the requirement for dynamic response of real active power tracking and the system stability jointly, a comprehensive parameter design is required. The value of k_i is selected to the maximum under meeting the damping ratio requirement.

C. Transient Synchronization Stability Assessment

According to Fig. 5, the PI controller is disabled when the fault is detected. The virtual power angle is defined as $\delta = \theta v{\rm ref} - \theta g$. In this case, the swing equation in the proposed method can be derived as

$$\begin{cases} \dot{\delta} = \omega - \omega_g \\ J\omega^*\dot{\omega} = P_{\rm ref} - P_{\rm vir} - D\omega^*(\omega - \omega^*) \end{cases} \tag{9}$$

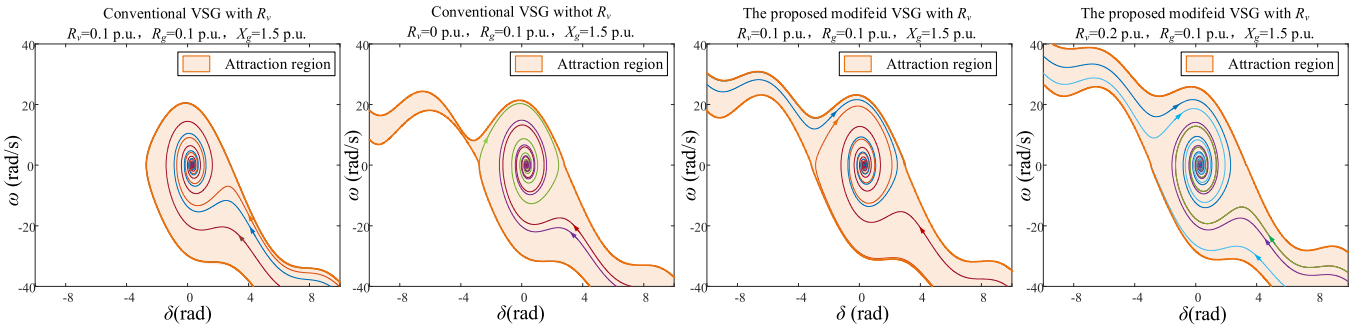

Fig. 9. Comparison of the attraction region between the basic VSG method with R_v and the proposed modified VSG control scheme with R_v.

where P_{vir} is expressed as

$$P_{\text{vir}} = \frac{3}{2}\frac{V_{v\text{ref}}^2(R_v+R_g)+V_{v\text{ref}}V_g[X_g\sin\delta-(R_v+R_g)\cos\delta]}{(R_v+R_g)^2+X_g^2}. \tag{10}$$

According to the swing (9), the attraction region can be obtained for transient stability assessment. Fig. 9 depicts the comparison of the attraction region between the conventional VSG method with R_v and the proposed method. The existence of R_v in conventional VSG narrows the attraction region, which means that R_v harms transient stability. The proposed method can greatly broaden the attraction region with the increase of virtual resistance R_v. The transient stability is greatly enhanced.

From the analysis mentioned above, the conflict between small-signal stability and transient stability due to virtual resistance is effectively solved under the proposed method. The existence of virtual resistance benefits both small-signal stability and transient synchronization stability under the modified VSG control scheme.

D. Qualitative Analysis on Frequency Regulation and Virtual Inertia Support

As one of the grid-forming control schemes, the proposed method is required to have the ability for frequency regulation and virtual inertia support.

Participating in frequency regulation refers to the ability that the grid-connected converter can adjust the output active power according to the grid frequency variation. Assuming that there is a grid frequency drop $\Delta\omega_g = 2\pi\Delta f_g$. According to (7), we have the following equation in steady-state:

$$P_e = P_{\text{ref}} - D\omega^*(\omega-\omega^*) \tag{11}$$

$$\omega = \omega_g - \Delta\omega_g \tag{12}$$

where ω^* is the same value as the nominal grid frequency ω_g.

Thus, the proposed modified VSG control scheme still has the P_e–f droop relationship and can achieve the primary frequency regulation.

Providing virtual inertia support refers to the ability that the grid-connected converter can suppress its maximum RoCoF (rate of change of frequency) to avoid triggering operation protection based on grid code during disturbances. Assuming that there is a step change of the power reference ΔP_{ref}. Usually, the maximum RoCoF is achieved when $t = 0$.

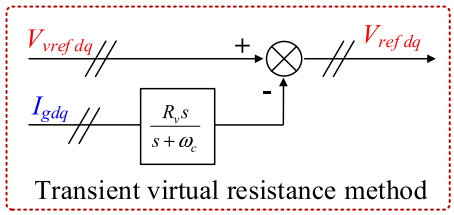

Fig. 10. Structure of the transient virtual resistance controller.

Thus, according to (7), the expression of maximum RoCoF can be derived as follows:

$$\left.\frac{\mathrm{d}\omega}{\mathrm{d}t}\right|_{\max} = \frac{(1+k_p)\Delta P_{\text{ref}}}{J\omega^*}. \tag{13}$$

From (13), the maximum RoCoF is determined by k_p and J. To avoid the negative impacts on frequency stability introduced by the proportional coefficient k_p, the value of k_p is selected to be no more than 0.2. Therefore, the proposed VSG control scheme can provide similar virtual inertia support to conventional VSG.

E. Compared With the Transient Virtual Resistance Method

To better illustrate the advantages of the proposed method, comparisons with the transient virtual resistance method [16], [34], [35] are carried out. The control structure of the transient virtual resistance method is shown in Fig. 10.

Fig. 11 shows the bode diagrams of the open-loop transfer function $\Delta P(s)/\Delta P_{\text{ref}}(s)$ under different methods. As indicated, the transient virtual resistance $R_v(s)$ is equivalent to R_v in the high-frequency region (nearly >100 Hz). $R_v(s)$ suppresses the resonance peak value and improves the small-signal stability. However, its performance of reducing resonance peak value is weaker than that of the proposed method.

Usually, the quasi-steady-state approximation is used to analyze transient stability [41]. The dynamics of the inner control loops are neglected due to their higher bandwidth [21]. As the transient virtual resistance $R_v(s)$ only affects the dynamics of the inner control loop, the function of $R_v(s)$ is equivalent to

$$\lim_{s\to 0} R_v(s) = \frac{R_v s}{s+\omega_c} = 0. \tag{14}$$

TABLE II
COMPARISON WITH THE EXISTING ADVANCED VSG METHODS

Methods	SR suppression	Transient stability	Influence of R_v	Complexity	Expansibility
Proposed scheme with R_v	Yes	√	√ Greatly enhances transient stability	Low	High
Conventional VSG with R_v	Yes	×	× Deteriorates transient stability	Low	High
Transient virtual impedance [16, 34, 35]	Yes	√	--- Limitedly improves transient stability	Low	High
Modify the control loop [21-23, 25-26, 28-29]	Needs R_v	√	× Deteriorates transient stability	Medium	Medium
Change the power reference [19, 27, 30-31]	Needs R_v	√	× Deteriorates transient stability	Low	Low
Co-design control parameters [20,24]	Needs R_v	√	× Deteriorates transient stability	High	High
Output impedance optimization [32]	Yes	√	× Deteriorates transient stability	High	Medium

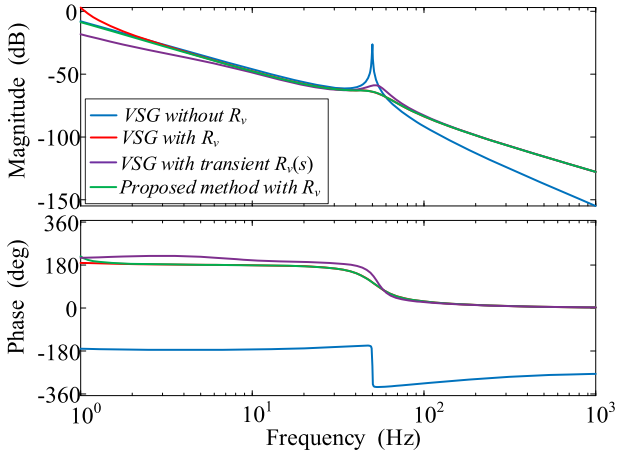

Fig. 11. Bode diagrams of the open-loop transfer function $\Delta P(s)/\Delta P_{ref}(s)$ under different control schemes with $R_v = 0.2$ p.u., $R_g = 0.05$ p.u., and $X_g = 1.5$ p.u.

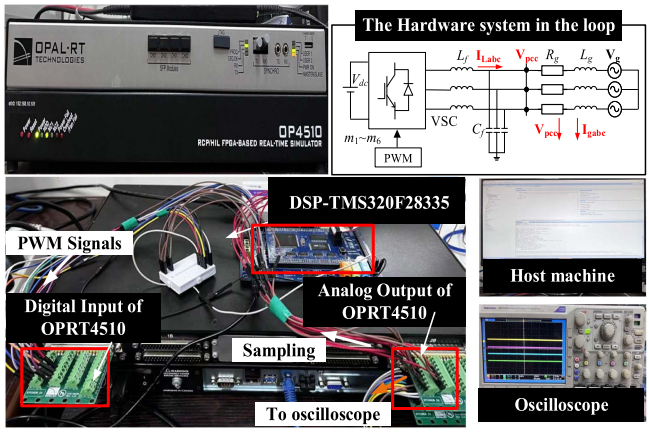

Fig. 12. Configuration of the control hardware-in-the-loop system.

In other words, the transient virtual resistance method is equivalent to the virtual resistance method with $R_v = 0$ from the perspective of transient synchronization stability. As discussed in [20], larger virtual resistance R_v will deteriorate the transient stability of VSG. Thus, the negative effect of $R_v(s)$ on the transient synchronization stability is trivial according to the above analysis, which also explains the reason why the transient stability of the transient virtual resistance method outperforms that of the virtual resistance method.

As indicated in (9), the effect of virtual resistance R_v in the proposed method on transient stability is equivalent to that of the grid resistance R_g. Because the grid resistance R_g could effectively enhance the transient stability of VSG [20], it is safe to say that the proposed method outperforms the transient virtual impedance method in terms of improving transient stability.

F. Compared With the Existing Advanced VSG Methods

To further illustrate the advantages of the proposed modified VSG control scheme, the comparisons between the proposed method and the existing methods are shown in Table II. The SR phenomena can be suppressed by adding virtual resistance. All the methods can improve the transient synchronization stability of VSG. However, only the proposed method and the transient virtual impedance method [10], [16], [34] can solve the conflict caused by virtual resistance between small-signal stability and transient stability. And the proposed method can greatly enhance transient stability. Besides, the implementation complexity of the proposed scheme is low and it has high expansibility to cooperate with other methods [19], [20], [21], [22], [23], [24], [25], [26], [27], [28], [29], [30], [31], [32]. Moreover, the ability for virtual inertia support and power-sharing regulation also remains.

IV. CONTROL HARDWARE-IN-LOOP EXPERIMENTAL VERIFICATION

To verify the effectiveness of the proposed modified VSG control scheme, experiments based on CHIL are carried out. The CHIL platform is shown in Fig. 12. The three-phase grid-connected converters, the *LC* filter, the line impedance, and the grid of the main circuit are emulated in the OPAL-RT4510 simulator. The controller of the converter is implemented in

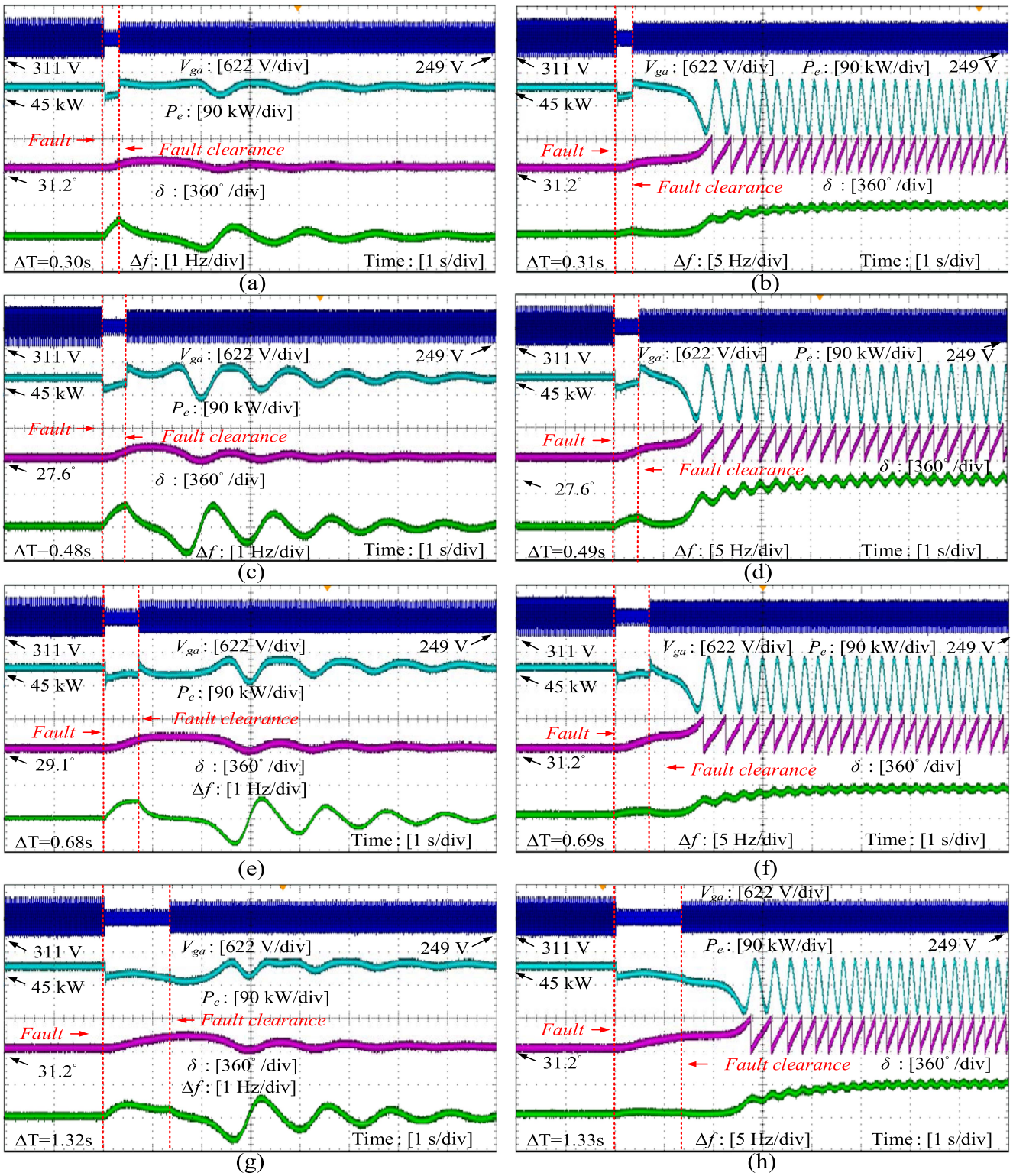

Fig. 13. CHIL experimental results under voltage sag. (a) Conventional VSG control with $R_v = 0.4\ \Omega$ under fault clearance time $\Delta T = 0.30$ s $= \mathrm{CCT}_1$. (b) Conventional VSG control with $R_v = 0.4\ \Omega$ under fault clearance time $\Delta T = 0.31$ s $> \mathrm{CCT}_1$. (c) Conventional VSG control with transient virtual impedance method, which integrates an HPF cascading with $R_v = 0.4\ \Omega$ under fault clearance time $\Delta T = 0.48$ s $= \mathrm{CCT}_2$. (d) Conventional VSG control with transient virtual impedance method, which integrates an HPF cascading with $R_v = 0.4\ \Omega$ under fault clearance time $\Delta T = 0.49$ s $> \mathrm{CCT}_2$. (e) Proposed modified VSG control scheme with $R_v = 0.2\ \Omega$ under fault clearance time $\Delta \mathrm{T} = 0.68$ s $= \mathrm{CCT}_3$. (f) Proposed modified VSG control scheme with $R_v = 0.2\ \Omega$ under fault clearance time $\Delta T = 0.69$ s $> \mathrm{CCT}_3$. (g) Proposed modified VSG control scheme with $R_v = 0.4\ \Omega$ under fault clearance time $\Delta T = 1.32$ s $= \mathrm{CCT}_4$. (h) Proposed modified VSG control scheme with $R_v = 0.4\ \Omega$ under fault clearance time $\Delta T = 1.33$ s $> \mathrm{CCT}_4$.

TABLE III
CHIL PARAMETERS

Parameters	Value	Parameters	Value
Grid voltage V_g	311 V	Rated active power P_{ref}	45 kW
Rated voltage V^*	325 V	Rated reactive power Q_{ref}	0
Grid frequency f_g	50 Hz	Virtual inertia J	6
Rated frequency f^*	50 Hz	Damping coefficient D	8
Line resistance R_g	0.05 Ω	Q-V loop coefficient n_q	0.001
Line inductance L_g	1.5 mH	Proportional coefficient k_p	0.05
C_f of LC filter	50 μF	Integral coefficient k_i	0.2
L_f of LC filter	1.2 mH	Virtual resistance R_v	0.4 Ω

the DSP-TMS320F28335 control board, and the sampling frequency is set to be 10 kHz. The experimental data is recorded by the host machine of OPAL-RT4510 and can be displayed through an oscilloscope. The experimental parameters are listed in Table III.

A. Transient Synchronization Stability Enhancement

To verify the effectiveness of transient stability enhancement, the large disturbance is selected as the grid voltage sag. When the fault occurs in this case, the grid voltage drops to 0.4 p.u. and after the fault is cleared, the grid voltage recovers to 0.8 p.u. of the normal condition. The CHIL experimental results are shown in Fig. 13.

Fig. 13(a) and (b) shows the waveforms of the conventional VSG control with $R_v = 0.4\ \Omega$ under different fault clearance times ΔT. Under such conditions, the critical fault clearance time CCT_1 is 0.30 s. Fig. 13(c) and (d) shows the waveforms under the transient virtual resistance method, which integrates an HPF cascading with $R_v = 0.4\ \Omega$. According to [16], ω_c is selected as 40. The critical fault clearance time CCT_2 is 0.48 s. Fig. 13(e) and (f) shows the waveforms under the proposed method with $R_v = 0.2\ \Omega$. The critical fault clearance time CCT_3 increases to 0.68 s. Fig. 13(g) and (h) shows the waveforms under the proposed method with $R_v = 0.4\ \Omega$. The critical fault clearance time CCT_4 increases to 1.32 s. Thus, it can be concluded that both the transient virtual resistance method and the proposed method could enhance the transient stability, the proposed method allowed longer CCT.

B. SR Suppression

To verify the effectiveness of SR suppression, a small disturbance of grid resistance change is considered in this case. The initial value of R_g is set as 0.2 Ω. After the system reached the steady state, R_g is changed to 0.05 Ω. Comparison CHIL experiments between conventional VSG and the proposed method with R_v are carried out.

Fig. 14(a) shows the CHIL experiment results under conventional VSG. When R_g is reduced from 0.2 to 0.05 Ω, SR phenomena occur in the curves of current, active power, and frequency. It may lead to potential instability for grid-forming control converters [18], [19]. Fig. 14(b) shows the results under the proposed method with $R_v = 0.4\ \Omega$. SR phenomena have been suppressed effectively. Therefore, the proposed method with virtual resistance can improve small-signal stability.

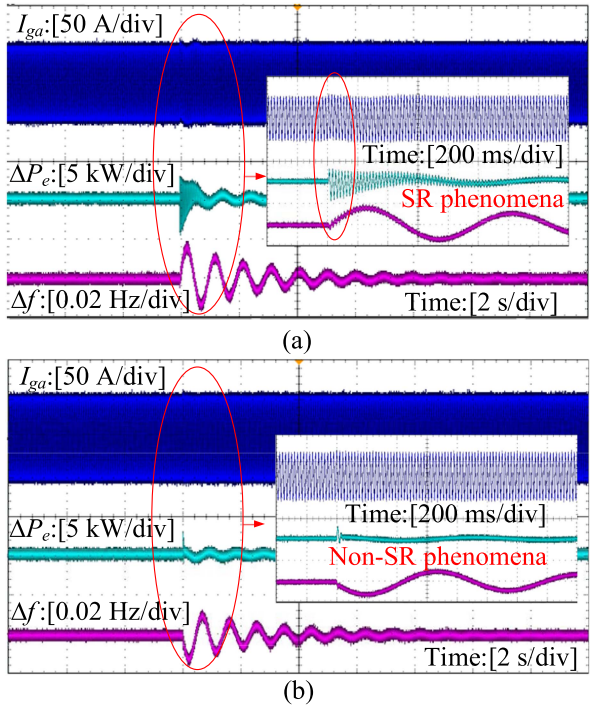

Fig. 14. CHIL experimental results for small-signal stability verification. (a) Conventional VSG control. (b) Proposed modified VSG control scheme with R_v.

C. Frequency Regulation and Inertia Supportability

The modified VSG control scheme should have the ability for frequency regulation and virtual inertia support under normal conditions. In this case, a 0.5 Hz drop in grid frequency has been considered. It is required that the output power should be regulated to increase to participate in the frequency regulation when a 0.5 Hz drop occurs. Fig. 15(a) shows the CHIL experimental results with the conventional VSG control and Fig. 15(b) shows the results with the proposed VSG control scheme. The proposed modified VSG control scheme can achieve similar control effects to conventional VSG in frequency regulation. Besides, the maximum RoCoF under the proposed method is about 2.21 Hz/s, which is close to it under the conventional VSG control. The proposed method hardly deteriorates the frequency stability.

D. Power-Sharing in Parallel Islanded Mode

In this case, two grid-forming converters are paralleled in islanded mode. The parameters are $J_1 = 6$, $J_2 = 10$, $D_1 = D_2 = 8$, $R_{g1} = R_{g2} = 0.05\ \Omega$, $L_{g1} = 1.5$ mH, $L_{g2} = 2.5$ mH, $R_{v1} = R_{v2} = 0.4\ \Omega$, $k_{p1} = k_{p2} = 0.05$, $k_{i1} = k_{i2} = 0.2$. The load increase of 30 kW is considered in this case. The result is shown in Fig. 16. Under the proposed modified VSG control, the power

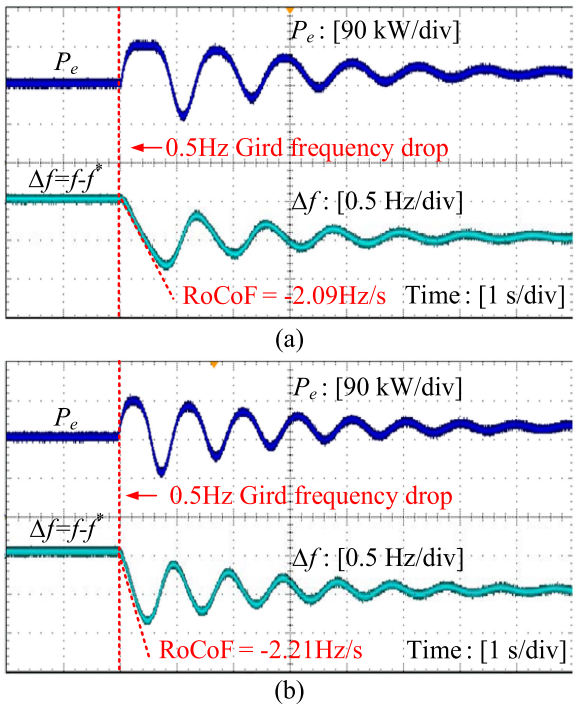

Fig. 15. CHIL experimental results under grid frequency drop. (a) Conventional VSG control. (b) Proposed modified VSG control scheme.

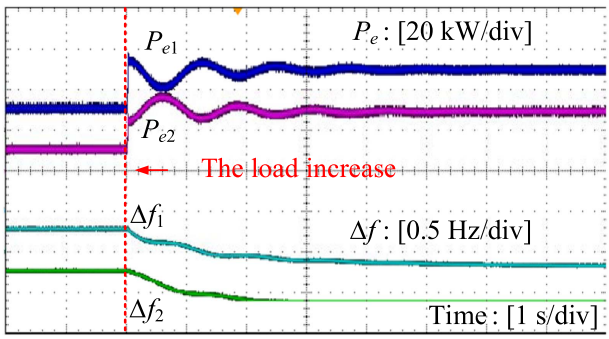

Fig. 16. CHIL experimental results of the proposed modified VSG control in parallel islanded mode.

sharing of the two paralleled converters in islanded mode can still be realized.

V. Conclusion

This article proposes a modified VSG control scheme with virtual resistance. Under this method, the conflict caused by virtual resistance between small-signal stability and transient stability is well solved. Besides, the proposed method still has the expansibility to cooperate with other enhanced methods. The ability for frequency regulation, virtual inertia support, and power-sharing regulation remains. Finally, CHIL experimental results verify the effectiveness of the proposed modified VSG control scheme.

Appendix

$$G_{P\delta}(s) = \frac{V_{v\mathrm{ref}}V_g(R_v+R_g+sL_g)\sin\delta_0+V_{v\mathrm{ref}}V_gX_g\cos\delta_0}{(R_v+R_g+sL_g)^2+X_g^2} - \frac{2V_{v\mathrm{ref}}V_gR_v\left[(R_v+R_g+sL_g)^2+X_g^2\right]\sin\delta_0}{(R_v+R_g+sL_g)^2+X_g^2} \tag{15}$$

$$G_{QV}(s) = \frac{V_{v\mathrm{ref}}V_gX_g\cos\delta_0-V_{v\mathrm{ref}}V_g(R_v+R_g+sL_g)\sin\delta_0}{(R_v+R_g+sL_g)^2+X_g^2} \tag{16}$$

$$G_{P_{\mathrm{vir}}\delta}(s) = \frac{V_{v\mathrm{ref}}V_g(R_v+R_g+sL_g)\sin\delta_0+V_{v\mathrm{ref}}V_gX_g\cos\delta_0}{(R_v+R_g+sL_g)^2+X_g^2}. \tag{17}$$

References

[1] F. Blaabjerg, R. Teodorescu, M. Liserre, and A. V. Timbus, "Overview of control and grid synchronization for distributed power generation systems," *IEEE Trans. Ind. Electron.*, vol. 53, no. 5, pp. 1398–1409, Oct. 2006.
[2] F. Milano, F. Dorfler, G. Hug, D. J. Hill, and G. Verbic, "Foundations and challenges of low-inertia systems (invited paper)," in *Proc. IEEE Power Syst. Comput. Conf.*, 2018, pp. 1–25.
[3] X. Fu et al., "Large-signal stability of grid-forming and grid-following controls in voltage source converter: A comparative study," *IEEE Trans. Power Electron.*, vol. 36, no. 7, pp. 7832–7840, Jul. 2021.
[4] J. Rocabert, A. Luna, F. Blaabjerg, and P. Rodríguez, "Control of power converters in AC microgrids," *IEEE Trans. Power Electron.*, vol. 27, no. 11, pp. 4734–4749, Nov. 2012.
[5] X. He, S. Pan, and H. Geng, "Transient stability of hybrid power systems dominated by different types of grid-forming devices," *IEEE Trans Energy Convers.*, vol. 37, no. 2, pp. 868–879, Jun. 2022.
[6] Q. C. Zhong and G. Weiss, "Synchronverters: Inverters that mimic synchronous generators," *IEEE Trans. Ind. Electron.*, vol. 58, no. 4, pp. 1259–1267, Apr. 2011.
[7] H. Bevrani, T. Ise, and Y. Miura, "Virtual synchronous generators: A survey and new perspectives," *Int. J. Elect. Power Energy Syst.*, vol. 54, pp. 244–254, 2014.
[8] J. Liu, Y. S. Miura, H. Bevrani, and T. Ise, "Enhanced virtual synchronous generator control for parallel inverters in microgrids," *IEEE Trans. Smart Grid*, vol. 8, no. 5, pp. 2268–2277, Sep. 2017.
[9] S. Chen, H. Han, X. Chen, Y. Sun, and X. Hou, "Reviews on inertia emulation technology with power electronics," in *Proc. IEEE Energy Convers. Congr. Expo.*, 2020, pp. 2101–2107.
[10] X. Wang, Y. W. Li, F. Blaabjerg, and P. C. Loh, "Virtual-impedance-based control for voltage-source and current-source converters," *IEEE Trans. Power Electron.*, vol. 30, no. 12, pp. 7019–7037, Dec. 2015.
[11] A S Vijay, N Parth, S Doolla, and M. C. Chandorkar, "An adaptive virtual impedance control for improving power sharing among inverters in islanded AC microgrids," *IEEE Trans. Smart Grid*, vol. 12, no. 4, pp. 2991–3003, Jul. 2021.
[12] M. G. Taul, X. Wang, P. Davari, and F. Blaabjerg, "Current limiting control with enhanced dynamics of grid-forming converters during fault conditions," *IEEE J. Emerg. Sel. Topics Power Electron.*, vol. 8, no. 2, pp. 1062–1073, Jun. 2020.
[13] X. Lin, Y. Zheng, Z. Liang, and Y. Kang, "The suppression of voltage overshoot and oscillation during the fast recovery process from load shortcircuit fault for three-phase stand-alone inverter," *IEEE J. Emerg. Sel. Topics Power Electron.*, vol. 9, no. 1, pp. 858–871, Feb. 2021.
[14] A. Rodríguez-Cabero, J. Roldán-Pérez, and M. Prodanovic, "Virtual impedance design considerations for virtual synchronous machines in weak grids," *IEEE J. Emerg. Sel. Topics Power Electron.*, vol. 8, no. 2, pp. 1477–1489, Jun. 2020.

[15] G. Li et al., "Analysis and mitigation of subsynchronous resonance in series-compensated grid-connected system controlled by a virtual synchronous generator," *IEEE Trans. Power Electron.*, vol. 35, no. 10, pp. 11 096–11 107, Oct. 2020.
[16] L. Zhang, L. Harnefors, and H. Nee, "Power-synchronization control of grid-connected voltage-source converters," *IEEE Trans. Power Syst.*, vol. 25, no. 2, pp. 809–820, May 2010.
[17] L. Harnefors, M. Hinkkanen, U. Riaz, F. M. M. Rahman, and L. Zhang, "Robust analytic design of power-synchronization control," *IEEE Trans. Ind. Electron.*, vol. 66, no. 8, pp. 5810–5819, Aug. 2019.
[18] J. Wang, Y. Wang, Y. Gu, W. Li, and X. He, "Synchronous frequency resonance of virtual synchronous generators and damping control," in *Proc. IEEE 9th Int. Conf. Power Electron.*, 2015, pp. 1011–1016.
[19] X. Wang, M. G. Taul, H. Wu, Y. Liao, F. Blaabjerg, and L. Harnefors, "Grid synchronization stability of converter-based resources—An overview," *IEEE Open J. Ind. Appl.*, vol. 1, pp. 115–134, Aug. 2020, doi: 10.1109/OJIA.2020.3020392.
[20] X. Xiong, C. Wu, and F. Blaabjerg, "Effects of virtual resistance on transient stability of virtual synchronous generators under grid voltage sag," *IEEE Trans. Ind. Electron.*, vol. 69, no. 5, pp. 4754–4764, May 2022.
[21] D. Pan, F. Liu, X.Wang, and R. Shi, "Transient stability of voltage-source converters with grid-forming control: A design-oriented study," *IEEE J. Emerg. Sel. Topics Power Electron.*, vol. 8, no. 2, pp. 1019–1033, Jun. 2020.
[22] X. Xiong, C. Wu, B. Hu, D. Pan, and F. Blaabjerg, "Transient damping method for improving the synchronization stability of virtual synchronous generators," *IEEE Trans. Power Electron.*, vol. 36, no. 7, pp. 7820–7831, Jul. 2021.
[23] R. Sun, J. Ma, W. Yang, S. Wang, and T. Liu, "Transient synchronization stability control for LVRT with power angle estimation," *IEEE Trans. Power Electron.*, vol. 36, no. 10, pp. 10 981–10 985, Oct. 2021.
[24] M. Choopani, S. H. Hosseinian, and B. Vahidi, "New transient stability and LVRT improvement of multi-VSG grids using the frequency of the center of inertia," *IEEE Trans. Power Syst.*, vol. 35, no. 1, pp. 527–538, Jan. 2020.
[25] X. Xiong, C. Wu, P. Cheng, and F. Blaabjerg, "An optimal damping design of virtual synchronous generators for transient stability enhancement," *IEEE Trans. Power Electron.*, vol. 36, no. 10, pp. 11 026–11 030, Oct. 2021.
[26] H. Wu and X. Wang, "A mode-adaptive power-angle control method for transient stability enhancement of virtual synchronous generators," *IEEE J. Emerg. Sel. Topics Power Electron.*, vol. 8, no. 2, pp. 1034–1049, Jun. 2020.
[27] P. Ge, F. Xiao, C. Tu, and Q. Guo, " Transient stability enhancement of a VSG based on flexible switching of control," in *Proc. CSEE*, vol. 42, no. 6, pp. 2109–2124, 2022.
[28] Z. Shuai, C. Shen, X. Liu, Z. Li, and Z. Shen, "Transient angle stability of virtual synchronous generators using Lyapunov's direct method," *IEEE Trans. Smart Grid*, vol. 10, no. 4, pp. 4648–4661, Jul. 2019.
[29] X. Xiong, C. Wu, and F. Blaabjerg, "An improved synchronization stability method of virtual synchronous generators based on frequency feedforward on reactive power control loop," *IEEE Trans. Power Electron.*, vol. 36, no. 8, pp. 9136–9148, Aug. 2021.
[30] M. Chen, D. Zhou, and F. Blaabjerg, "Enhanced transient angle stability control of grid-forming converter based on virtual synchronous generator," *IEEE Trans. Ind Electron.*, vol. 69, no. 9, pp. 9133–9144, Sep. 2022.
[31] K. Sun, W. Yao, J. Wen, and L. Jiang, "A two-stage simultaneous control scheme for the transient angle stability of VSG considering current limitation and voltage support," *IEEE Trans. Power Syst.*, vol. 37, no. 3, pp. 2137–2150, May 2022.
[32] D. Pan, X. Wang, F. Liu, and R. Shi, "Transient stability impact of reactive power control on grid-connected converters," in *Proc. IEEE Energy Convers. Congr. Expo.*, 2019, pp. 4311–4316.
[33] S. P. Me, S. Zabihi, F. Blaabjerg, and B. Bahrani, "Adaptive virtual resistance for postfault oscillation damping in grid-forming inverters," *IEEE Trans. Power Electron.*, vol. 37, no. 4, pp. 3813–3824, Apr. 2022.
[34] A. D. Paquette and D. M. Divan, "Virtual impedance current limiting for inverters in microgrids with synchronous generators," *IEEE Trans. Ind. Appl.*, vol. 51, no. 2, pp. 1630–1638, Mar./Apr. 2015.
[35] X. Zhang et al., "Analysis of dynamic power angle oscillation and its suppression strategy for the droop-controlled grid-connected inverter," *IEEE J. Emerg. Sel. Topics Power Electron.*, vol. 9, no. 5, pp. 5718–5731, Oct. 2021, doi: 10.1109/JESTPE.2021.3078290.
[36] L. Huang, H. Xin, Z. Wang, L. Zhang, K. Wu, and J. Hu, "Transient stability analysis and control design of droop-controlled voltage source converters considering current limitation," *IEEE Trans. Smart Grid*, vol. 10, no. 1, pp. 578–591, Jan. 2019.
[37] H. Geng, L. Liu, and R. Li, "Synchronization and reactive current support of PMSG-based wind farm during severe grid fault," *IEEE Trans. Sustain. Energy.*, vol. 9, no. 4, pp. 1596–1604, Oct. 2018.
[38] S. F. Zarei, H. Mokhtari, and F. Blaabjerg, "Fault detection and protection strategy for islanded inverter-based microgrids," *IEEE J. Emerg. Sel. Topics Power Electron.*, vol. 9, no. 1, pp. 472–484, Feb. 2021.
[39] I. Sadeghkhani, M. E. H. Golshan, A. Mehrizi-Sani, J. M. Guerrero, and A. Ketabi, "Transient monitoring function-based fault detection for inverter-interfaced microgrids," *IEEE Trans. Smart Grid.*, vol. 9, no. 3, pp. 2097–2107, May 2018.
[40] E. Casagrande, W. L. Woon, H. H. Zeineldin, and D. Svetinovic, "A differential sequence component protection scheme for microgrids with inverter–based distributed generators," *IEEE Trans. Smart Grid.*, vol. 5, no. 1, pp. 29–37, Jan. 2014.
[41] X. Wang and H. -D. Chiang, "Quasi steady-state model for power system stability: Limitations, analysis and a remedy," in *Proc. Power Syst. Comput. Conf.*, 2014, pp. 1–7, doi: 10.1109/PSCC.2014.7038362.